Available at www.sciencedirect.com

ScienceDirect

journal homepage: www.elsevier.com/locate/watres

A biofilm model for prediction of pollutant transformation in sewers

Feng Jiang[a,b], *Derek Hoi-wai Leung*[c], *Shiyu Li*[b], *Guang-Hao Chen*[c,*], *Satoshi Okabe*[d], *Mark C.M. van Loosdrecht*[e]

[a]School of Chemistry and Environment, South China Normal University, Guangzhou, China
[b]School of Environmental Science & Engineering, Sun Yat-sen University, Guangzhou, China
[c]Department of Civil Engineering, The Hong Kong University of Science and Technology, Clear Water Bay, Kowloon, Hong Kong, China
[d]Department of Environmental Engineering, Hokkaido University, Hokkaido, Japan
[e]Department of Biotechnology, Delft University of Technology, Julianalaan 67, NL-2628 BC Delft, The Netherlands

ARTICLE INFO

Article history:
Received 21 October 2008
Received in revised form
16 April 2009
Accepted 21 April 2009
Published online 6 May 2009

Keywords:
Sewer
Biofilm model
Spatial concentration profile
Heterotrophs, Autotrophs and sulfate-reducing bacteria
Model verification and application

ABSTRACT

This study developed a new sewer biofilm model to simulate the pollutant transformation and biofilm variation in sewers under aerobic, anoxic and anaerobic conditions. The biofilm model can describe the activities of heterotrophic, autotrophic, and sulfate-reducing bacteria (SRB) in the biofilm as well as the variations in biofilm thickness, the spatial profiles of SRB population and biofilm density. The model can describe dynamic biofilm growth, multiple biomass evolution and competitions among organic oxidation, denitrification, nitrification, sulfate reduction and sulfide oxidation in a heterogeneous biofilm growing in a sewer. The model has been extensively verified by three different approaches, including direct verification by measurement of the spatial concentration profiles of dissolved oxygen, nitrate, ammonia, and hydrogen sulfide in sewer biofilm. The spatial distribution profile of SRB in sewer biofilm was determined from the fluorescent *in situ* hybridization (FISH) images taken by a confocal laser scanning microscope (CLSM) and were predicted well by the model.

1. Introduction

Sewer biofilms play an important role in pollutant transformation in sewers (Chen et al., 2003). Nielsen and Hvitved-Jacobsen (1988) reported that anaerobic conditions developed in deep parts of sewer biofilms promoted hydrogen sulfide production, leading to sewer odor and corrosion problems. Competition among chemical oxygen demand (COD) oxidation, nitrification, denitrification and sulfate reduction could occur in the biofilms in sewers when oxygen and/or nitrate are injected. A comprehensive biofilm model, therefore, is necessary to describe all reactions and competitions. However, sulfate-reducing bacteria (SRB) have always been ignored in existing biofilm models, though heterotrophs and nitrifiers have already been considered (Picioreanu et al., 2004; Rauch et al., 1999; Wanner and Gujer, 1986; Wanner and Reichert, 1996). While sulfide production has been considered in some sewer models, such as the wastewater aerobic/anaerobic transformation in sewers (WATS) model (Hvitved-Jacobsen et al., 2000), variations in SRB density, sulfate concentration and substrate diffusion in sewer biofilms have commonly been neglected, suggesting that such models do

* *Corresponding author.*
E-mail address: ceghchen@ust.hk (G.-H. Chen).
0043-1354/$ – see front matter © 2009 Elsevier Ltd. All rights reserved.
doi:10.1016/j.watres.2009.04.043

Nomenclature

Δt	time interval for computation (s)
P_k	percentage of SRB in segment k to total amount of SRB in the entire biofilm
Δz	height of biofilm compartment (m)
$b_{A,NO}$	anoxic endogenous respiration of nitrifiers (d^{-1})
R_k	number of SRB cell in the biofilm segment k
$b_{A,O2}$	aerobic endogenous respiration of nitrifiers (d^{-1})
q_{fe}	Fermentation rate constant (d^{-1})
$b_{H,NO}$	anoxic endogenous respiration rate of X_H (d^{-1})
S_A	fermentation product (g COD m^{-3})
$b_{H,O2}$	aerobic endogenous respiration rate of X_H (d^{-1})
S_F	fermentable substrate (g COD m^{-3})
b_{INA}	inactivation rate constant (d^{-1})
S_{H2S}	dissolved sulfide (g S m^{-3})
b_{SRB}	decay rate constant of SRB (d^{-1})
S_{NH}	ammonium and ammonia nitrogen (g N m^{-3})
$b_{STO,NO}$	anoxic respiration rate for X_{STO} (d^{-1})
S_{NO}	nitrate and nitrite (g N m^{-3})
$b_{STO,O2}$	aerobic respiration rate for X_{STO} (d^{-1})
S_O	dissolved oxygen (g O_2 m^{-3})
D_f	the diffusion coefficient in biofilm (m^2 s^{-1})
S_S	readily biodegradable substrate (g COD m^{-3}) = $S_F + S_A$
D_w	the diffusion coefficient in water (m^2 s^{-1})
S_{SO4}	sulfate (g SO_4–S m^{-3})
f_{XI}	production of X_I in endogenous biomass respiration (g X_I g^{-1} X_H)
V	stoichiometric matrix
X_A	nitrifiers (g COD m^{-3})
i_{NBM}	nitrogen content of active biomass (g N g^{-1} $X_{biomass}$)
X_H	heterotrophic biomass (g COD m^{-3})
i_{NSf}	nitrogen content of S_F (g N g^{-1} S_S)
X_I	Inert organic particulates (g COD m^{-3})
i_{NXI}	nitrogen content of X_I (g N g^{-1} X_I)
X_S	slowly biodegradable substrate (g COD m^{-3})
i_{NXS}	nitrogen content of X_S (g N g^{-1} X_S)
X_{SRB}	sulfate-reducing bacteria (g COD m^{-3})
J	diffusion flux (g m^{-2} s^{-1})
X_{STO}	storage product of X_H (g COD m^{-3})
$K_{A,NH}$	S_{NH} saturation constant for nitrifiers (g Nm^{-3})
Y_A	yield of nitrifers per g NO_3–N (g COD g^{-1} N)
$K_{A,O}$	oxygen saturation constant for nitrifiers (g O_2 m^{-3})
$Y_{H,NOx}$	anoxic yield of heterotrophic growth on X_{STO}
k_{att}	attachment coefficient (d^{-1}) (g X_H g^{-1} X_{STO})
k_{det}	detachment coefficient (g m^{-5})
$Y_{H,O2}$	aerobic yield of heterotrophic growth on X_{STO}
K_{fe}	S_F saturation constant for fermentation (gCOD m^{-3}) (g X_H g^{-1} X_{STO})
k_H	hydrolysis rate constant (g X_S g^{-1} X_{-H} d^{-1})
Y_{SRB}	Yield of SRB (g X_{SRB} g^{-1} S_A)
k_La	re-aeration coefficient in 20 °C (s^{-1})
$Y_{STO,NOx}$	anoxic yield of stored products per S_s
K_{NH}	saturation constant for S_{NH} (g N m^{-3}) (g X_{STO} g^{-1} S_S)
K_{NO}	saturation constant for S_{NO} (g N m^{-3})
$Y_{STO,O2}$	Aerobic yield of stored products per S_s
K_{O2}	saturation constant for oxygen (g O_2 m^{-3}) (g X_{STO} g^{-1} S_S)
K_S	saturation constant for substrate S_S (g S_S m^{-3})
ε_l	volume fraction of liquid
K_{SA}	S_A saturation constant for SRB growth (g S_A m^{-3})
$\varepsilon_{X_{ij}^f}$	fraction of particulate i in biofilm compartment j
k_{SO}	sulfide oxidation rate constant ($(gO_2m^{-3})^{-0.1}$ d^{-1})
η_{NO}	anoxic reduction factor
K_{SO4}	sulfate saturation constant for SRB growth(g S m^{-3})
μ_A	autotrophic maximum growth rate (d^{-1})
$K_{SRB,O}$	oxygen inhibition constant for SRB growth(g O_2 m^{-3})
μ_H	heterotrophic maximum aerobic growth rate (d^{-1})
k_{STO}	aerobic storage rate constant (g S_S g^{-1} X_H d^{-1})
μ_{SRB}	growth rate constant of SRB (d^{-1})
K_{STO}	saturation constant for storage (g X_{STO} g^{-1} X_H)
ρ_b^f	maximum density for active biomass (X_H, X_{STO}, X_A and X_{SRB}) (kg COD m^{-3})
K_X	hydrolysis saturation constant (g X_S g^{-1} X_H)
k_ε	constant for calculating ε_l
ρ_r^f	maximum density for residuals (X_S and X_I) (kg COD m^{-3})
l	conservation matrix of COD and nitrogen
L_f	biofilm thickness (m)
ρ_m	mass density of biofilm (g TS m^{-3})
M_i	mass of particulate i in the whole biofilm (g m^{-3})
τ_w	wall shear stress (N m^{-2})
M_{TSS}	mass of whole biofilm (g m^{-3})

not predict the dynamic evolution of bacterial populations and the dynamic development of biofilm in sewers. This means that WATS does not evaluate hydrogen sulfide production and in sewer denitrification when nitrate is dosed under various conditions. Sharma et al. (2008) proposed a new sewer model to simulate H_2S production, but this model neglects the effect of sewer biofilms. They concluded that the spatial variation of biofilm activities should be considered and their model needs further improvement in this aspect.

On the other hand, if a comprehensive sewer biofilm model has been established, it would be difficult to verify it because the current verification methods rely upon external mass balances alone (Buffiere et al., 1998; Horn et al., 2003; Tsuno et al., 2002). This is mainly due to the fact that direct verification involving measurement of spatial concentration profiles of multiple substrates and products in a sewer biofilm requires micro-sensoring and molecular microbiological techniques. However, recent advances in the development of microelectrodes (Kühl and Jørgensen, 1992; Noguera et al., 1999) and the fluorescent *in situ* hybridization (FISH) technique enable us to determine spatial concentration profiles of various substrates and bacterial population distributions within a biofilm (Okabe et al., 2003). Hence, by combining these techniques, we measured the spatial concentration profiles of NH_4^+, NO_3^-, NO_2^-, H_2S, pH, and dissolved oxygen (DO) within a sewer biofilm (Leung et al., 2004).

With the above in view, this study aimed at developing a new sewer biofilm model to describe the competitions among heterotrophs, autotrophs and sulfate-reducing bacteria in a sewer biofilm to predict denitrification, COD removal, and hydrogen sulfide production in sewers and to consider the dynamic evolution of the biofilms under various conditions. We calibrated and validated this new model through three comparisons between the model simulations and the measurements of: (1) the biofilm growth in sewers; (2) the biomass density variation in the biofilms; and (3) the spatial concentration profiles of multiple substances and the population distribution of SRB in the biofilms.

2. Model development

2.1. Spatial structure

The main differences in the biofilm structures and properties within a sewer are in the development of the biofilm in the direction away from walls of the sewer pipe. The direction through the biofilm is described as ''vertical'' and the biofilm model developed here will simulate the vertical differences inside the sewer biofilms as well as the substance exchanges between the bulk water and the biofilms. There could be many layers in the biofilm in this vertical direction. The distance between such two layers is labeled ''Δz'', as shown in Fig. 1, and can be variable as shown in Table 2, with varying biofilm density in each layer or compartment along the biofilm depth. As the value of Δz determines the amount of the biofilm compartments; the accuracy, computation time and instability of the calculation would increase with decreasing Δz. In the calculation trials, a $\Delta z < 0.05$ mm induced the divergence of the diffusion computation while a $\Delta z > 0.15$ mm resulted in the insufficiency of calculation accuracy. Therefore Δz in the small range of 0.05 ~ 0.15 mm, satisfies the balance of the accuracy, computation time and stability of the calculation.

2.2. Processes and variables

Based on the ''diffusion-reaction'' concept (Wanner and Gujer, 1986), our model describes the spatial concentration variations of seven solutes (S_i) and six particulates (X_i) in each compartment of the biofilm (see Table 1). To evaluate the mass density of each compartment, the total solid (TS) is determined from all particulate concentrations in the compartment, following the typical conversion parameters proposed in the International Water Association's (IWA) Activated Sludge Model No. 3 (ASM3) (IWA, 2000). The re-aeration process was activated only when the calculation involved the bulk water. A sewer biofilm engages in three physical processes responsible for mass exchanges between each compartment and that between the biofilm and bulk water phases. It considers 21 biochemical processes depending on the concentrations of the soluble and particulate substances. The details of the key processes are as follows.

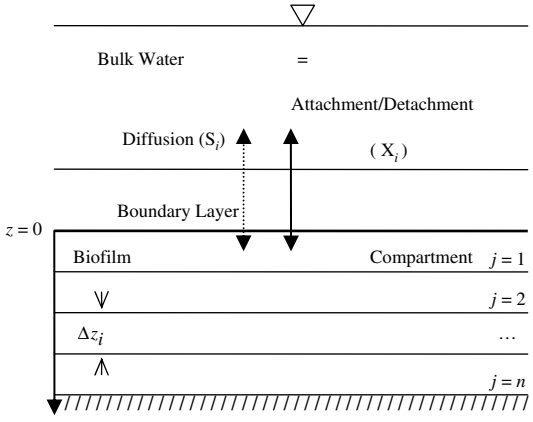

Fig. 1 – Schematic representation of the model biofilm for a sewer biofilm system.

2.2.1. Sewer biofilm attachment and detachment

Microbial adhesion to the sewer biofilm surface is regarded as a necessary step in biofilm formation (Wuert et al., 2003). Detachment of sewer biofilms is of importance in sewer biofilm modeling, though it is often overlooked in biotreatment systems (Wuert et al., 2003). However, in a sewer environment where the sewage quality significantly varies along the sewer line over time, the attachment and detachment of the biofilms need to be taken into consideration in the modeling (Chen and Leung, 2000). Huisman and Gujer (2002) proposed Eqs. (1) and (2) to evaluate the rates of the attachment and detachment of sewer biofilms. These two equations are adopted in this study. Since the detachment equation is only suitable for a homogenous biofilm (Huisman and Gujer, 2002), the detached mass is thus reallocated by Eq. (3) to suit a non-homogeneous sewer biofilm.

$$r_{att,X_i^w} = k_{att} \cdot X_i^w, \tag{1}$$

where

i = substance index;
r_{att,X_i^w} = attachment rate of particulate i (g COD m^{-3} d^{-1});
X_i^w = *concentration of particulate i* in the bulk water phase (g COD m^{-3}); and
k_{att} = attachment coefficient (d^{-1})

$$r_{det,X_i^w} = k_{det}\mu_H L_f^2 \left(\frac{\tau_w - \tau_w^{min}}{\tau_w^{min}}\right)^{2.5} \tanh\left(\frac{M_i}{M_{TSS}}\right) \tag{2}$$

$$r_{det,X_{i,j}^f} = -r_{det,X_i^w} \cdot X_{i,j}^f / \sum_{j=1}^{n} X_{i,j}^f \tag{3}$$

where

j = biofilm compartment index; n is max j;
r_{det,X_i^w} = *detachment rate of particulate* i into the bulk water phase (g COD m^{-3} d^{-1});
$r_{det,X_{i,j}^f}$ = *detachment rate of particulate i from biofilm compartment j* (g COD m^{-3} d^{-1});
$X_{i,j}^f$ = *concentration of particulate i in biofilm compartment j* (*g COD* m^{-3});
k_{det} = *detachment coefficient* (g m^{-5});
μ_H = maximum heterotrophic growth rate (d^{-1}),
L_f = biofilm thickness (m);

Table 1 – Stoichiometric and conservation matrix for the biochemical process model for gravity sewers.

	Variable index (i)	1	2	3	4	5	6	7	8	9	10	11	12	13	Rate
	Model component	S_O	S_F	S_A	S_{NH}	S_{NO}	S_{SO4}	S_{H2S}	X_I	X_S	X_H	X_{STO}	X_A	X_{SRB}	
	Unit ($g\ m^{-3}$)	COD	COD	COD	N	N	S	S	COD	COD	COD	COD	COD	COD	
k	*Stoichiometric matrix ($\upsilon_{k,j}$)*														
1	Hydrolysis		x_1		y_1					-1					$k_H \frac{X_S/X_H}{K_X+X_S/X_H} X_H$
2	Aerobic storage of S_S	x_2	$-S_F/(S_F+S_A)$	$-S_A/(S_F+S_A)$	y_2							$Y_{STO,O2}$			$k_{STO} \cdot \frac{S_O}{K_O+S_O} \cdot \frac{S_F+S_A}{K_S+S_F+S_A} \cdot X_H$
3	Anoxic storage of S_S		$-S_F/(S_F+S_A)$	$-S_A/(S_F+S_A)$	y_3	x_3						$Y_{STO,NOx}$			$k_{STO} \cdot \eta_{NO} \cdot \frac{K_O}{K_O+S_O} \cdot \frac{S_{NO}}{K_{NO}+S_{NO}} \cdot \frac{S_F+S_A}{K_S+S_F+S_A} \cdot X_H$
4	Aerobic growth of X_H	x_4			y_4						1	$-1/Y_{H,O2}$			$\mu_H \cdot \frac{S_O}{K_O+S_O} \cdot \frac{S_{NH}}{K_{NH}+S_{NH}} \cdot \frac{X_{STO}/X_H}{K_{STO}+X_{STO}/X_H} \cdot X_H$
5	Anoxic growth of X_H				y_5	x_5					1	$-1/Y_{H,NOx}$			$\eta_{NO} \cdot \mu_H \cdot \frac{K_O}{K_O+S_O} \cdot \frac{S_{NO}}{K_{NO}+S_{NO}} \cdot \frac{S_{NH}}{K_{NH}+S_{NH}} \cdot \frac{X_{STO}/X_H}{K_{STO}+X_{STO}/X_H} \cdot X_H$
6	Aerobic end. respiration for X_H	x_6			y_6				f_{XI}		-1				$b_{H,O2} \cdot \frac{S_O}{K_O+S_O} \cdot X_H$
7	Anoxic end. respiration for X_H				y_7	x_7			f_{XI}		-1				$b_{H,NO} \cdot \frac{K_O}{K_O+S_O} \cdot \frac{S_{NO}}{K_{NO}+S_{NO}} \cdot X_H$
8	Aerobic respiration for X_{STO}	x_8										-1			$b_{STO,O2} \cdot \frac{S_O}{K_O+S_O} \cdot X_{STO}$
9	Anoxic respiration for X_{STO}					x_9						-1			$b_{STO,NO} \cdot \frac{K_O}{K_O+S_O} \cdot \frac{S_{NO}}{K_{NO}+S_{NO}} \cdot X_{STO}$
10	Nitrification	x_{10}			y_{10}	$1/Y_A$							1		$\mu_A \cdot \frac{S_O}{K_{A,O}+S_O} \cdot \frac{S_{NH}}{K_{A,NH}+S_{NH}} \cdot X_A$
11	Aerobic end. respiration for X_A	x_{11}			y_{11}				f_{XI}				-1		$b_{A,O2} \cdot \frac{S_O}{K_O+S_O} \cdot X_A$
12	Anoxic end. respiration for X_A				y_{12}	x_{12}			f_{XI}				-1		$b_{A,NO} \cdot \frac{K_O}{K_O+S_O} \cdot \frac{S_{NO}}{K_{NO}+S_{NO}} \cdot X_A$
13	SRB growth			-1	y_{13}		$-x_{13}$	x_{13}						Y_{SRB}	$\mu_{SRB} \frac{K_{SRB,O}}{K_{SRB,O}+S_O} \frac{S_{SO4}}{K_{SO4}+S_{SO4}} \frac{S_A}{K_{SA}+S_A} X_{SRB}$
14	SRB decay				y_{14}				1					-1	$b_{SRB} X_{SRB}$
15	Heterotrophs inactivation				y_{15}				1		-1				$k_{ina} \frac{K_S}{K_S+S_F+S_A} X_H$
16	Storage product inactivation			1								-1			$k_{ina} \frac{K_S}{K_S+S_F+S_A} X_{STO}$
17	Autotrophs inactivation				y_{17}				1				-1		$k_{ina} \frac{K_O}{K_O+S_O} X_A$
18	SRB inactivation				y_{18}				1					-1	$k_{ina} \frac{S_O}{K_{SRB,O}+S_O} X_{SRB}$
19	Sulfide oxidation	x_{19}					1	-1							$k_{SO} \cdot S_o^{0.1} \cdot S_{H2S}$
20	Fermentation		-1	1	y_{20}										$q_{fe} \frac{K_O}{K_O+S_O} \frac{K_{NO}}{K_{NO}+S_{NO}} \frac{S_F}{K_{fe}+S_F} X_H$
21	Re-aeration	1													$k_L a \cdot (S_{O,sat} - S_O)$
	Conservation matrix														
1	COD ($l_{1,j}$)	-1	1			-4.57		2	1	1	1	1	1	1	
2	Nitrogen ($l_{2,j}$)		i_{NSf}		1	1			i_{NXI}	i_{NXS}	i_{NBM}		i_{NBM}	i_{NBM}	

τ_w = wall shear stress (N m^{-2});
τ_w^{min} = minimal wall shear stress (N m^{-2});
M_i = mass of particulate i in the whole biofilm in a cross section (g m^{-3}); and
M_{TSS} = mass of whole biofilm in a cross section (g m^{-3}).

2.2.2. Solute diffusion

Diffusion fluxes of the solutes in a biofilm can be determined by Eq. (4). As the substrates do not penetrate through a sewer pipe wall, the boundary conditions for the substrate diffusion can be described by Eq. (5),

$$J_{i,j} = -D_{f,i,j}\frac{\partial S_{i,j}}{\partial y_j} \quad (4)$$

$$J_{i,n} = 0 \quad (5)$$

where

y = coordinate of the vertical direction (m);
$S_{i,j}$ = *concentration of solute i in a biofilm compartment j* (g m^{-3});
$J_{i,j}$ = *diffusion flux of solute i into a biofilm compartment j* (g m^{-2} s^{-1}); and
$D_{f,i,j}$ = diffusion coefficient of solute i in biofilm (m^2 s^{-1}).

$D_{f,i,j}$ can be calculated from the sewer biofilm mass density and the diffusion coefficient of solute i in water ($D_{w,i}$) following Eq. (6) (Fan et al., 1990):

$$D_{f,i,j} = D_{w,i}\cdot\left(1 - \frac{0.43\rho_{m,j}^{0.92}}{11.19 + 0.27\rho_{m,j}^{0.99}}\right) \quad (6)$$

where $\rho_{m,j}$ = mass density of a biofilm compartment j (g TS m^{-3}).

In the above, the diffusion through the diffusive boundary layer can be determined by Eq. (4), while the thickness of the hydraulic boundary layer can be determined from the mean water depth and the Sherwood number which depends on the shear velocity and water viscosity (Dawson and Trass, 1972).

2.2.3. Biochemical processes

The ASM3 model is suitable to model the main biochemical processes in a sewer biofilm (Huisman and Gujer, 2002; Jiang et al., 2006). To describe the sulfate reduction process in sewer biofilms, readily biodegradable substrates cover the aggregate of fermentable substrates (S_F) and the fermentation products (S_A) (mainly volatile fatty acids, VFAs). S_A is considered as only electron donor of sulfate reduction in this study. Hence, the fermentation process is included in our sewer biofilm model. In order to simulate the formation of inactive organic materials, such as extra-cellular polymer substances (EPS), the bacterial inactivation equations proposed by Horn et al. (2003) and Wanner and Reichert (1996) are adopted in this study. S_A is assumed to be the inactivation product of the storage products (X_{STO}). The stoichiometry and kinetics of sulfate reduction and sulfide oxidation used in this study are based on relevant previous studies (Nielsen and Hvitved-Jacobsen, 1988; Nielsen et al., 2005; Okabe et al., 2003). They are integrated into the extended ASM3, as shown in Table 1. In Table 1, the stoichiometric parameters, x_k and y_k are calculated from $\sum_{i=1}^{13} \upsilon_{k,i}\cdot l_{1,i} = 0$ and $\sum_{i=1}^{13} \upsilon_{k,i}\cdot l_{2,i} = 0$ where $\upsilon_{k,i}$ is the value of the stoichiometric matrix in line k, column i, and $l_{1,i}$ or $l_{2,i}$ is the value of the conservation matrix in line 1 or 2, column i. Temperature effect on the reaction rates of the biochemical processes is determined by Eq. (7).

$$r = r_{20}\cdot\theta_T^{(T-20)} \quad (7)$$

Where

T = *temperature* (°C);
r = reaction rate of any biochemical process at temperature T (g COD, S, N or O_2 m^{-3} d^{-1});
r_{20} = reaction rate of any biochemical process at 20 °C (g COD, S, N or O_2 m^{-3} d^{-1}); and
θ_T = temperature coefficient. This parameter value is available in the literature (Hvitved-Jacobsen et al., 1998).

2.3. Density determination

To simulate heterogeneity in a sewer biofilm, our model regards the mass density of the biofilm as a variable. In any biofilm compartment, this density can be determined from the volumetric fractions of particulates, which are the fractions of every particulate and liquid in the compartments, as describe by Eq. (8).

$$\varepsilon_l + \sum_{i=1}^{n} \varepsilon_{X_{i,j}^f} = 1 \quad (8)$$

where

ε_l = *volume fraction of the liquid;*
$\varepsilon_{X_{i,j}^f}$ = *volume fraction of the particulate i in the biofilm;*
ε_l and $\varepsilon_{X_{i,j}^f}$ are calculated by Eqs. (9) and (10), respectively (Horn and Hempel, 1997).

$$\varepsilon_l = 0.2 + \left(\frac{k_\varepsilon}{500 * 0.25^{\left(10^3/(10^6 z+1)\right)} + 1}\right) \quad (9)$$

$$\varepsilon_{X_{i,j}^f} = \frac{X_{i,j}^f}{\rho_i^f}, \quad (10)$$

where

k_ε = *a constant that can be found in the literature* (Horn and Hempel, 1997);
ρ_i^f = maximum density of particulate i in the biofilm (g COD m^{-3}), which is shown in Table 2.

3. Experimental methods and materials

To calibrate and validate our sewer biofilm model, experiments, including biofilm thickness measurement in sewer, internal microelectrode measurement and SRB vertical distribution measurement of biofilms were conducted. Sewage quality transformation in a real sewer section was also investigated to obtain the data necessary for simulation and application of the model.

Table 2 – Summary of the parameter values used in the model for conversions in a gravity sewer.

Symbol	Value	Unit	Reference	Symbol	Value	Unit	Reference
Model parameter				q_{fe}	3.0	d^{-1}	(IWA, 2000)
Δz	0.5 ~ 1.5	10^{-4} m	–	K_{fe}	20	g COD m^{-3}	(IWA, 2000)
Δt	1	S	–	μ_A	1	d^{-1}	(IWA, 2000)
ρ_b^f	60	kg COD m^{-3}	Calibrated	$K_{SRB,O}$	0.1	g O_2 m^{-3}	(Nielsen et al., 2005)
ρ_r^f	200	kg COD m^{-3}	(Laspidou and Rittmann, 2004)	K_{SO4}	6.4	g S m^{-3}	(Ingvorsen et al., 1984)
k_e	0.5	–	(Horn and Hempel, 1997)	b_{SRB}	0.192	d^{-1}	(Moosa et al., 2002)
Kinetic parameter				b_{INA}	0.028	d^{-1}	(Horn et al., 2003)
k_H	9.53	d^{-1}	(Jiang et al., 2007)	k_{SO}	1×10^5	(g O_2 m^{-3})$^{-0.1}$ d^{-1}	(Nielsen et al., 2006)
K_X	4.76	g X_S g^{-1} X_H	〃	μ_{SRB}	0.8	d^{-1}	Calibrated
k_{STO}	4.94	d^{-1}	〃	K_{SA}	0.1	g S_A m^{-3}	Calibrated
η_{NO}	0.51	–	〃	k_{att}	1×10^{-2}	d^{-1}	Calibrated
K_O	1.88	g O_2 m^{-3}	〃	k_{det}	1.4×10^7	g m^{-5}	Calibrated
K_{NO}	2.00	g N m^{-3}	〃			*Stoichiometric parameter*	
K_S	15.2	g COD m^{-3}	〃	f_{XI}	0.2	g X_I g^{-1} X_H	(Jiang et al., 2007)
K_{STO}	2.04	g X_{STO} g^{-1} X_H	〃	$Y_{STO,O2}$	0.82	g X_{STO} g^{-1} S_S	〃
μ_H	2.50	d^{-1}	〃	$Y_{STO,NOx}$	0.69	g X_{STO} g^{-1} S_S	〃
K_{NH}	0.01	g N m^{-3}	〃	$Y_{H,O2}$	0.70	g X_H g^{-1} X_{STO}	〃
$b_{H,O2}$	0.17	d^{-1}	〃	$Y_{H,NOx}$	0.55	g X_H g^{-1} X_{STO}	〃
$b_{H,NO}$	0.19	d^{-1}	〃	Y_A	0.24	g COD g^{-1} N	〃
$b_{STO,O2}$	0.17	d^{-1}	〃	i_{NSI}	0.01	g N g^{-1} S_I	〃
$b_{STO,NO}$	0.19	d^{-1}	〃	i_{NSf}	0.020	g N g^{-1} S_F	〃
$K_{A,NH}$	0.68	g N m^{-3}	〃	i_{NXI}	0.037	g N g^{-1} X_I	〃
$K_{A\ O}$	0.63	g O_2 m^{-3}	〃	i_{NXS}	0.024	g N g^{-1} X_S	〃
$b_{A,O2}$	0.16	d^{-1}	〃	i_{NBM}	0.050	g N g^{-1} $X_{biomass}$	〃
$b_{A,NO}$	0.05	d^{-1}	〃	Y_{SRB}	0.596	g X_{SRB} g^{-1} S_A	(Moosa et al., 2002)

〃: means the same with above.

3.1. *Sewer biofilm growth measurement*

To calibrate and validate the proposed biofilm model, a 90 day biofilm growth experiment was conducted in the sewer section of the Hong Kong University of Science and Technology (HKUST). As shown in Fig. 2, the sewer section is a 1.5 km long cement pipe with an inner diameter of 0.45 m and a slope of 0.0075. Sewer biofilms were developed on specially designed PVC chips (3 × 3 cm) that were installed in the sewer. The chips could be removed for weekly measurement of the biofilm thickness. Biofilm samples taken from the sewer section were fixed by incubation in paraformaldehyde (4% [wt/vol] in phosphate-buffered saline, PBS) at 4 °C for 8–12 h, embedded in Tissue-Tek OCT compound (Miles, Elkhart, Ind.) and frozen at −20 °C. Vertical thin sections (10–20 μm thick) of the fixed samples were prepared as described by Ramsing et al. (1993). The average thickness of the sewer biofilm was obtained from at least three measurements of the vertical thin slices under the electronic microscope. The thickness became stable after 8 weeks (see Fig. 3), indicating biofilms reached a steady-state. Hence, the biofilms grown for 2 months were sampled and subjected to an average mass density measurement by measuring its total solids content at 105 °C (APHA, 1995) as well as biofilm thickness.

3.2. *Microelectrode measurement within biofilm*

To obtain information on the spatial concentration profiles of some soluble substances, we measured the spatial concentration profile of the soluble substances sulfide, oxygen, ammonium, nitrate/nitrite in the sewer biofilm using microelectrode measurements. The biofilm samples were collected for the microelectrode measurement. Multiple microelectrodes were applied to measure the profiles under favorable conditions. The biofilm sample on the PVC chip was taken into laboratory and acclimated at 25 °C in the synthetic medium for 8 h before the measurements were initiated to ensure steady-state profiles. The synthetic medium consisted of NO_2^- (50 μM), NO_3^- (50 μM), NH_4Cl (200 μM), Na_2SO_4 (2000 μM), Na_2HPO_4 (3000 μM), $MgCl_2$ $6H_2O$ (84 μM), $CaCl_2$ (200 μM), EDTA

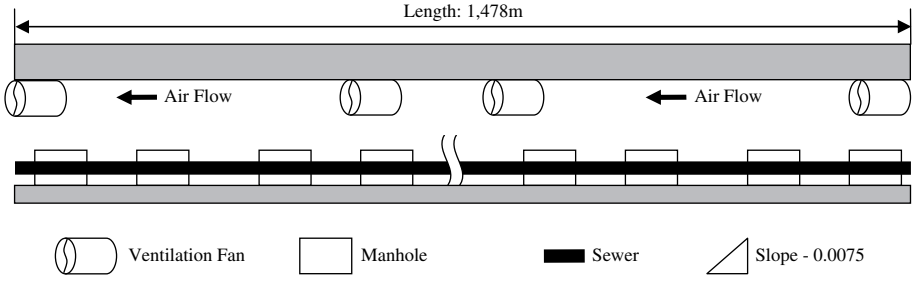

Fig. 2 – Schematic diagram of the sewer at the site of the Hong Kong University of Science and Technology.

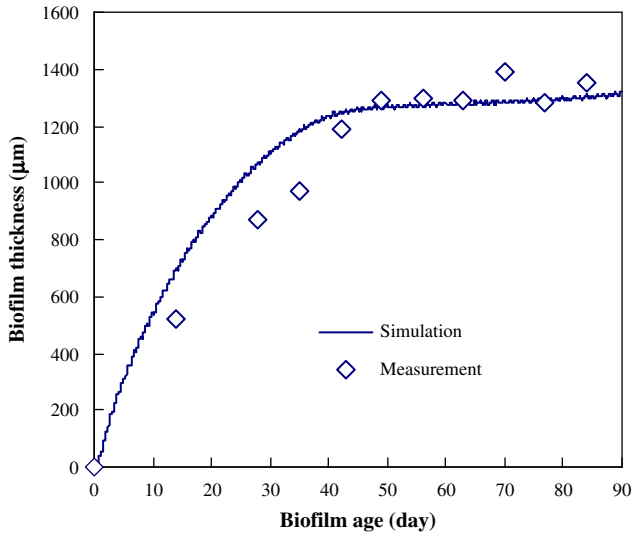

Fig. 3 – Comparison of simulated and measured development of the thickness of a sewer biofilm.

(270 μM), Yeast (0.1 g), Peptone (0.1 g). The pH was at 7.08. The dissolved oxygen level was maintained at 6–6.5 mg/L. The volume of the bulk liquid was two liters. Steady-state concentration profiles of O_2, NH_4^+, NO_3^-, NO_2^-, H_2S and pH in the biofilms were recorded according to the protocol reported in Satoh et al. (2003) and Okabe et al. (2003). Clark-type microelectrodes for O_2 and H_2S with a tip diameter of approximately 15 μm were calibrated. H_2S electrode, and liquid ion-exchanging membrane microelectrodes for measurements of pH, NO_2^-, NO_3^-, NH_3, O_2 were employed.

3.3. *Determination of the vertical distribution of SRB in biofilms*

FISH and confocal laser scanning microscope (CLSM) techniques are useful in obtaining information on bacterial populations in biofilms (Ito et al., 2002). Using these techniques with a SRB385 probe allows the spatial distribution of SRB in a biofilm to be obtained (Okabe et al., 1999b). Two biofilm samples grown on the PVC chips in the HKUST sewer for 2 months were collected, fixed and subsequently washed twice in PBS for *in situ* hybridization. After the fixation, the biofilm samples were cut into slices and examined under an LSM 510 confocal laser scanning microscope (Carl Zeiss) equipped with an argon laser (488 nm), a HeNe laser (543 nm), and a UV laser (364 nm). Images were recorded by using simultaneous excitation of the 488 and 543 nm lasers to distinguish the probe-stained cells from debris and minerals after the background signal level was adjusted (Okabe et al., 1999a). All images were combined, processed, and analyzed with a standard software package provided by Zeiss. A percentile profile of the SRB population along the biofilm depth was then obtained through image analysis using MATLAB 7.0 After counting the number of red pixels (R) on all images of every biofilm layer, the percentile profile of the SRB in the entire biofilm can be derived from

$$P_k = R_k / \sum_{k=1}^{m} R_k \quad (11)$$

where

k = the index of vertical biofilm segments in the CLSM images;
m = the maximum number of biofilm segments in the CLSM measurements; and
P_k = the percentage of SRB in segment k in relation to the total amount of SRB in the entire biofilm.

3.4. *Sewer sewage quality experiment*

In situ 3 h online DO monitoring was performed at both the inlet and outlet of the HKUST sewer section, during which sewage samples were taken at both sites for analysis. Total COD was determined and the COD components were measured by the respirometric method to determine the COD fractions (Petersen et al., 2003). NH_4–N and NOx–N were determined using a flow injection analyzer (FIA) (Quikchem). The details of the experiment and analysis were reported by Jiang et al. (2006, 2007).

4. Results and discussion

4.1. *Model simulation*

To simulate biofilm growth in the HKUST sewer, the data of the hydraulics and sewage quality which obtained in our previous studies were used. The details were reported in our previous studies (Chen and Leung, 2000; Jiang et al., 2006, 2007; Leung, 2000). Typical 24 h variations of the flow rate ranging from 1.1 to 1.8 m/s and the DO concentration ranging from 3 to 6 mg/L at the sewer inlet (Chen and Leung, 2000) were applied. The 24 h variation data of total organic carbon (TOC) ranged from 8 to 100 mg/L (Chen and Leung, 2000). The ratio of COD to DOC and the COD fractions for all kinds of organisms (Jiang et al., 2006) formed a 24 h variable boundary condition for the dynamic model simulation on sewage quality variations in the sewer. A mean sulfate concentration was set at 236.7 mgSO_4–S/L in the incoming sewage according to our previous study (Leung, 2000). Based on the conditions above, the model was programmed with Visual FORTRAN 6.5.

4.2. *Model calibration and validation*

The values of the biokinetic and stoichiometric parameters of our biofilm model are mainly drawn from our previous study (Jiang et al., 2007) with some obtained from the literature (Horn et al., 2003; Laspidou and Rittmann, 2004; Moosa et al., 2002; Nielsen et al., 2005, 2006; Okabe et al., 1992), except a few parameters determined through the model calibration, as shown in Table 2. To calibrate our model, the 90 day biofilm thickness profile was used to determine the attachment coefficient k_{att} and the detachment coefficient k_{det}, and the SRB spatial distribution profiles obtained by CLSM were used to determine the parameters related to sulfate reduction. For both internal and external validation, we used the measured average biofilm

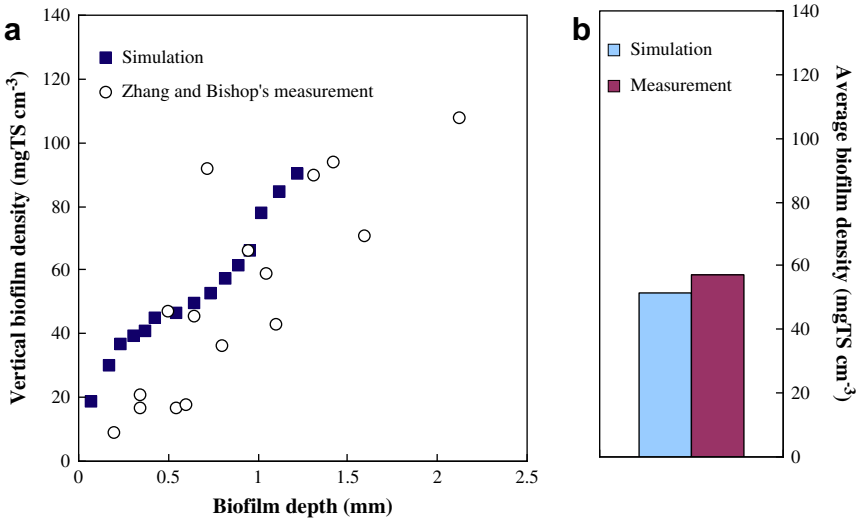

Fig. 4 – Comparison of model simulation with: (a) the reported measurements (Zhang and Bishop, 1994) of spatial variation in biofilm density (the origin of x-axis means the water/biofilm interface); and (b) the measured average biofilm density of the biofilm grown in HKUST sewer.

densities, the spatial variations of biofilm density reported by Zhang and Bishop (1994), four simultaneous spatial concentration profiles of DO, NH_4–N, NO_X–N and sulfide in the biofilm, as well as the *in situ* online DO profiles of the sewer section.

4.2.1. *Calibration with the biofilm thickness in the sewer*

The rate coefficients of biofilm attachment and detachment were determined from 90 day model simulation results that can reflect the measured thickness of the sewer biofilm. The biofilm thickness profile and the corresponding simulation result are shown in Fig. 3. The biofilm thickness initially increased with biofilm age and then became stable after 8 weeks, which was predicted by our model after calibration.

4.2.2. *Verification with the data on biofilm density*

To compare the proposed model with the measured average biofilm density and the spatial density profiles, Zhang and Bishop (1994)'s data were employed. In both their experiments and our study, the biofilms were cultured on removable strips under aerobic conditions. The COD level used in their experiments was also close to that of the sewage in our sewer. Furthermore, the simulation was made for steady-state biofilms. We, therefore, believe that Zhang and Bishop's biofilm density data could be useful for verification of our sewer biofilm model.

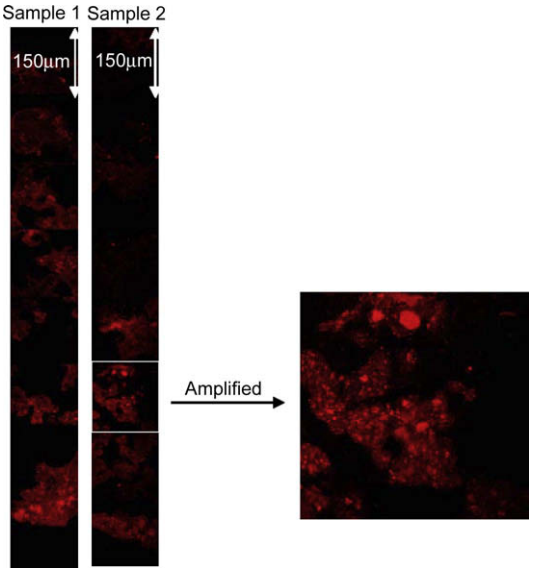

Fig. 5 – Confocal laser scanning microscope (CLSM) images of the sewer biofilms labeled with SRB385 RNA-probe, illustrating the distribution of sulfate-reducing bacteria along the depth of the sewer biofilm.

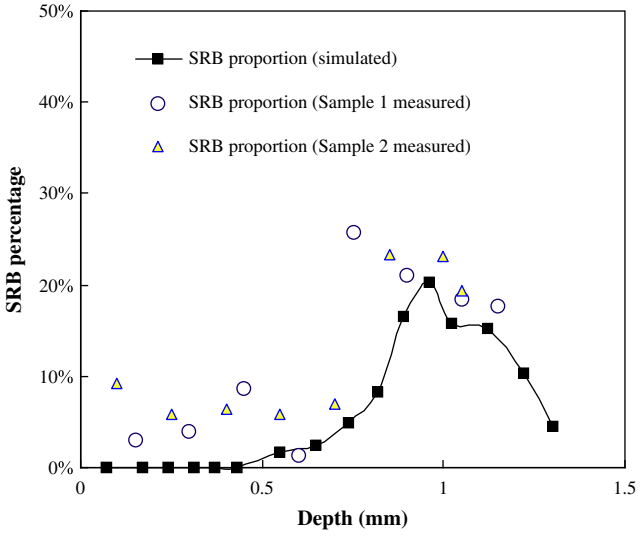

Fig. 6 – Model simulation and measurement of the distribution of sulfate-reducing bacteria over the depth in the biofilm (the origin of x-axis means the water/biofilm interface).

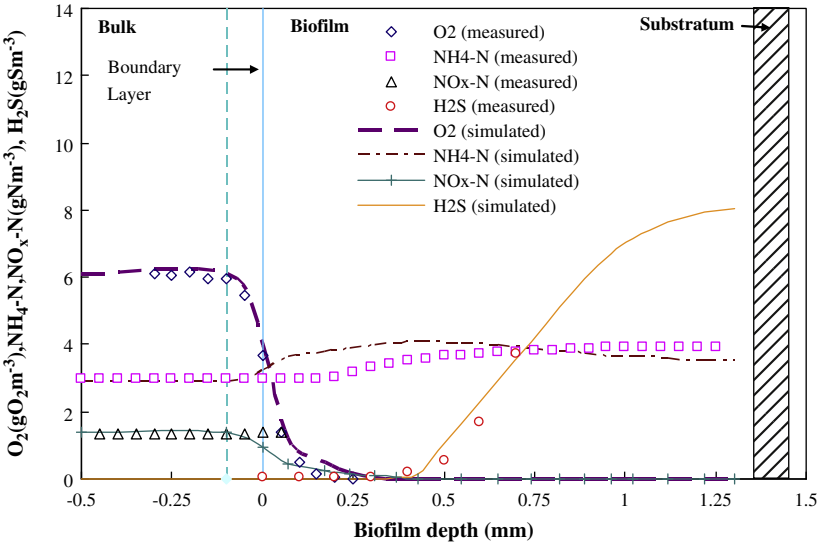

Fig. 7 – Model simulation and measurements of the spatial concentration profiles over the biofilm depth of dissolved oxygen (g O_2 m^{-3}), ammonium, nitrate/nitrite (g N m^{-3}) and sulfide (g S m^{-3}).

The average density of the biofilm sample taken from the HKUST sewer was determined to be 57 mg TS cm^{-3} while the model simulation result was 51.6 mg TS cm^{-3}, as revealed in Fig. 4b, and the comparison of the reported experimental data with our model predictions on biofilm density profile is shown in Fig. 4a. The simulation conditions applied to a steady-state sewer biofilm grown in the gravity sewer with a steep slope of 0.0075 where minimum DO is 3 mg/L (Chen and Leung, 2000). Apparently, the proposed model predicted well the average biofilm density. The simulated density profile along biofilm depth is also closed to the reported density profile, though the simulated density is slightly higher than the reported data, which may be due to the difference of hydraulic conditions between two experiments. The biofilm density profile demonstrates the heterogeneity of biofilm, and this feature is important because the sewer hydraulic and sewage quality conditions of a sewer usually significantly fluctuate, thus resulting in spatial non-uniformity of sewer biofilms. Since biofilm density is closely related to porosity, this result also reveals that the calibrated model has potential to simulate biofilm porosity and spatial structures along the depth direction as well.

4.2.3. *Calibration with the vertical SRB distribution data*

To investigate sulfate reduction along the biofilm depth, vertical SRB distributions in the sewer biofilms were determined. The CLSM images, as shown in Fig. 5, of the sewer biofilm samples were used to analyze the percentile profiles of SRB along the biofilm depth. The results were used for model calibration to determine μ_{SRB} and K_{SA}, and the simulated and measured results are shown in Fig. 6. After calibration, the model simulations basically agreed with the measurements of the SRB profile along the biofilm depth, indicating that the proposed biofilm model is able to simulate the transformation of microbes in a sewer biofilm. As revealed by this figure, the SRB concentration in the bottom layers of the biofilm decreased, indicating that the sulfate reduction rate was limited due to the insufficiency of substrates in deep biofilm layers.

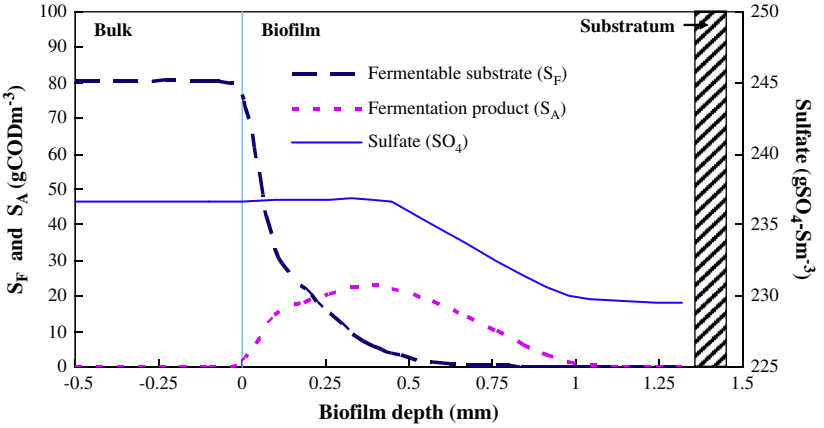

Fig. 8 – Simulated concentration profiles of fermentable substrate (S_F), fermentation products (S_A) and sulfate in the sewer biofilm at the peak time of COD loading (3 pm).

4.2.4. *Verification by spatial profiles of soluble substances*

To confirm the validity of the proposed model, concentration profiles of the multiple solutes measured by microelectrodes were used. As far as we know, this is the first time that direct verification of a biofilm model by comparison of model simulations with the measurements of four simultaneous spatial concentration profiles of DO, NH_4–N, NO_X–N and sulfide in a biofilm has been attempted. The results are shown in Fig. 7. The model's predictions agreed with the measurements of all the spatial concentration profiles, confirming that the proposed model can predict the quantitative behaviors of ammonia, oxygen, nitrate and sulfide in a sewer biofilm. This further demonstrates that the developed model, incorporating the extended ASM3 model with the proposed bio-kinetics for sulfate reduction and sulfide oxidation describes the competition among the different types of biomass involving organic oxidation, nitrification, denitrification, and sulfate reduction in a sewer biofilm.

Our previous study (Leung et al., 2004) found that the sewer biofilms contain a significant amount of SRB. This was further confirmed in this study by the sharp increase of hydrogen sulfide concentration with biofilm depth, in particular at the depth of 0.5–1 mm, as shown in Fig. 7. This could be because of the SRB increasing due to a completed penetration of sulfate into the biofilm when oxygen and nitrate/nitrite only penetrate to a depth of less than 0.25 mm depth. This finding was close to the results from previous studies using microelectrode, even if the sulfate concentration were significantly lower than that in this study (Kühl and Jørgensen, 1992; Okabe et al., 2003), which indicating the sulfate concentration could be not the limited factor for sulfide production in biofilms. Air injection can help control H_2S production in sewers (Zhang et al., 2008), but Fig. 7 shows that even if the sewage is under an aerobic conditions (DO >6 mg/L), sulfide production remains high in the deep parts of the biofilm. This implies that the injecting air to control H_2S mainly contributed to increasing the sulfide oxidation rate, rather than decreasing the sulfate reduction rate.

As indicted by Fig. 8, after a depth of 1 mm substrates became limited for sulfate reduction even while the COD of influent sewage was of its peak time in 24 h variation. As a result, the sulfide production rate decreased in the deeper parts of biofilm. This phenomenon is in accord with the findings in the measurements and simulation results of the spatial SRB distribution in Fig. 6.

The above simulation results reveal that the proposed model is able to simulate the transformation and transportation of not only solutes and but also particulates in the biofilms in a sewer.

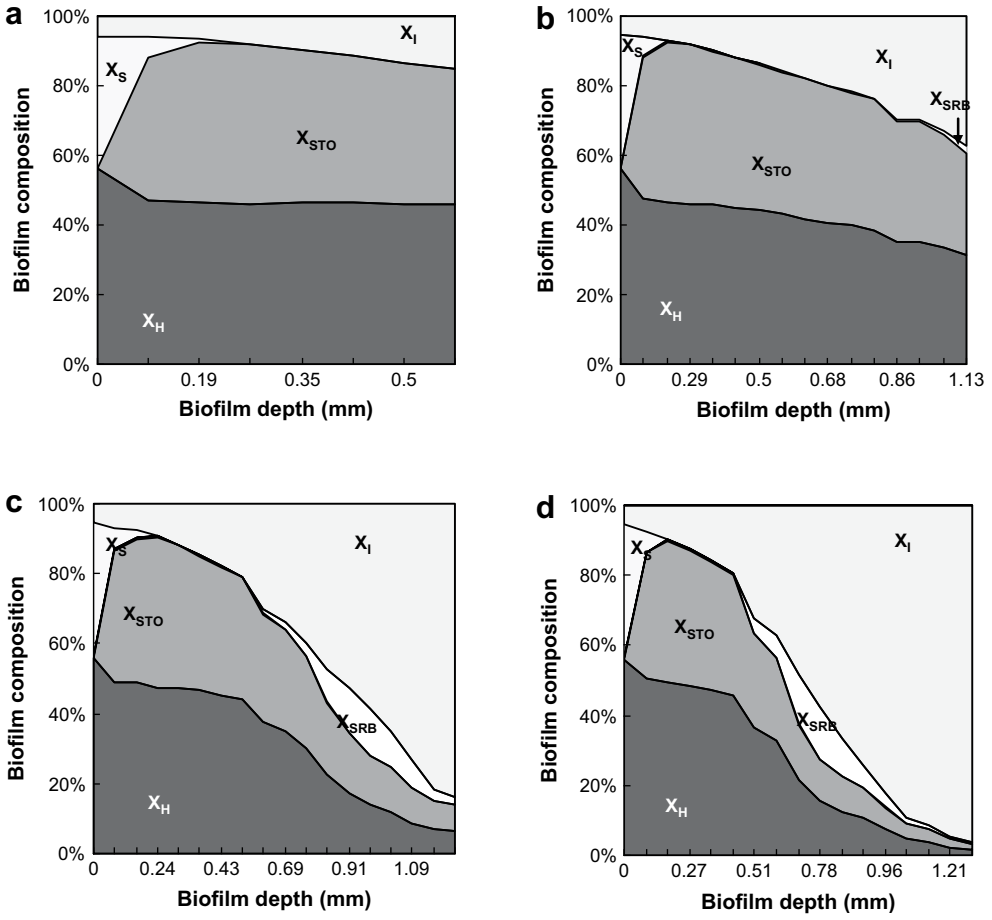

Fig. 9 – Simulated microbial populations of the sewer biofilm at different time after initiation of biofilm growth: (a) 10th; (b) 30th; (c) 60th; and (d) 90th day (the origin of x-axis means the water/biofilm interface).

4.3. *Model application*

The proposed model after calibration and verification was conducted to evaluate the bacterial competition and biofilm evolution in the sewer. In the simulation of biofilm growth in the HKUST sewer section, the biofilm showed a distinct evolution due to bacterial competition. Fig. 9 shows that bacterial competition in the biofilm induces evolution during a 90 day growth period. Heterotrophic bacteria existed exclusively in the first 10 days of growth (see Fig. 9a); SRB appeared in the deep layers at 30 days (see Fig. 9b). This is because DO was absent in these layers. With increasing biofilm thickness, SRB grew rapidly and occupied larger fractions of the biofilm (see Fig. 9c). After 2 months of growth, the biofilm became stable and the SRB percentage increased slightly (see Fig. 9d). A reduction in the SRB fraction in the bottom layers was mainly attributed to the penetration limit of substrate. It should be noted that nitrifiers (X_A) almost disappeared in the sewer biofilm, indicating that nitrifiers completely failed to compete with other microbes in the biofilm.

5. Conclusions

This study developed a comprehensive biofilm model to predict pollutant transformation and biofilm growth in sewer biofilms. The main conclusions drawn from this study are as follows:

(1) The model is able to describe dynamic biofilm growth, multiple biomass evolution and competition among organic oxidation, denitrification, nitrification, sulfate reduction and sulfide oxidation in heterogenic biofilms in sewers.
(2) The model has been extensively verified using different approaches, particularly direct verification with measurements of the spatial concentration profiles of DO, nitrate/nitrite, ammonia, and sulfide in a sewer biofilm.
(3) The spatial distribution profile of SRB in the sewer biofilm was also analyzed using FISH images taken under a CLSM. The predictions agreed well with the image analysis.

Acknowledgements

The authors acknowledge financial support from the Hong Kong Research Grants Council (611606), the National Natural Science Foundation of China (50808088), and Guangdong Natural Science Foundation (8451063101001185). We thank Drs. T.C. Zhang and P.L. Bishop for allowing us to cite their biofilm density measurements published in Water Research 28(11), 2267–2277.

REFERENCES

APHA, 1995. Standard Methods for Water and Wastewater Examination. American Public Health Association, Washington, D.C.

Buffiere, P., Steyer, J.P., Fonade, C., Moletta, R., 1998. Modeling and experiments on the influence of biofilm size and mass transfer in a fluidized bed reactor for anaerobic digestion. Water Research 32 (3), 657–668.

Chen, G.H., Leung, D.H.W., 2000. Utilization of oxygen in a sanitary gravity sewer. Water Research 34 (15), 3813–3821.

Chen, G.H., Leung, D.H.W., Hung, J.C., 2003. Biofilm in the sediment phase of a sanitary gravity sewer. Water Research 37 (11), 2784–2788.

Dawson, D.A., Trass, O., 1972. Mass transfer at rough surfaces. International Journal of Heat and Mass Transfer 15, 1317.

Fan, L.S., Leyva-Ramos, R., Wisecarver, K.D., Zehner, B.J., 1990. Diffusion of phenol through a biofilm grown on activated carbon particles in a draft-tube three-phase fluidized-bed bioreactor. Biotechnology and Bioengineering 35 (3), 279–286.

Horn, H., Hempel, D.C., 1997. Substrate utilization and mass transfer in an autotrophic biofilm system: experimental results and numerical simulation. Biotechnology and Bioengineering 53 (4), 363–371.

Horn, H., Reiff, H., Morgenroth, E., 2003. Simulation of growth and detachment in biofilm systems under defined hydrodynamic conditions. Biotechnology and Bioengineering 81 (5), 607–617.

Huisman, J.L., Gujer, W., 2002. Modelling wastewater transformation in sewers based on ASM3. Water Science and Technology 45 (6), 51–60.

Hvitved-Jacobsen, T., Vollertsen, J., Nielsen, P.H., 1998. A process and model concept for microbial wastewater transformations in gravity sewers. Water Science and Technology 37 (1), 233–241.

Hvitved-Jacobsen, T., Vollertsen, J., Tanaka, N., 2000. An integrated aerobic/anaerobic approach for prediction of sulfide formation in sewers. Water Science and Technology 41 (6), 107–115.

Ingvorsen, K., Zehnder, A.J., Jorgensen, B.B., 1984. Kinetics of sulfate and acetate uptake by *Desulfobacter postgatei*. Applied and Environmental Microbiology 47 (2), 403–408.

Ito, T., Nielsen, J.L., Okabe, S., Watanabe, Y., Nielsen, P.H., 2002. Phylogenetic identification and substrate uptake patterns of sulfate-reducing bacteria inhabiting an oxic-anoxic sewer biofilm determined by combining microautoradiography and fluorescent in situ hybridization. Applied and Environmental Microbiology 68 (1), 356–364.

IWA, 2000. Activated sludge models ASM1, ASM2, ASM2d, and ASM3. IWA Publishing, London.

Jiang, F., Leung, H.W.D., Li, S.Y., Lin, G.S., Chen, G.H. (2006). Use of genetic algorithm to calibrate activated sludge model no. 3-based sewer process model. In: Proceedingsof the Second IWA International Conference on Sewer Operation and Maintenance, 26–28 October, Vienna, Austria.

Jiang, F., Leung, H.W.D., Li, S.Y., Lin, G.S., Chen, G.H., 2007. A new method for determination of parameters in sewer pollutant transformation process model. Environmental Technology 28 (11), 1217–1225.

Kühl, M., Jørgensen, B.B., 1992. Microsensor measurements of sulfate reduction and sulfide oxidation in compact microbial communities of aerobic biofilms. Applied and Environmental Microbiology 58 (4), 1164–1174.

Laspidou, C.S., Rittmann, B.E., 2004. Modeling the development of biofilm density including active bacteria, inert biomass, and extracellular polymeric substances. Water Research 38 (14–15), 3349–3361.

Leung, D.H.W. (2000) Study of oxygen utilization and dissolved organic removal in a sanitary gravity sewer. M.Phil dissertation, The Hong Kong University of Science and Technology, Hong Kong.

Leung, H.W.D., Chen, G.H., Ito, T., Okabe, S., Watanabe, Y., 2004. Comparison of community structure of sulfate-reducing bacteria and their roles in carbon mineralization in sewer

biofilms growing under aerophilic and microaerophilic conditions. In: Proceedingsof the IWA Specialized International Conference on Biofilms, 24–16 October, Las Vegas, Nevada.

Moosa, S., Nemati, M., Harrison, S.T.L., 2002. A kinetic study on anaerobic reduction of sulphate. Part I: effect of sulphate concentration. Chemical Engineering Science 57 (14), 2773–2780.

Nielsen, A.H., Hvitved-Jacobsen, T., 1988. Effect of sulfate and organic matter on hydrogen sulfide formation in biofilms of filled sanitary sewers. Journal Water Pollution Control Federation 60 (5), 627–634.

Nielsen, A.H., Yongsiri, C., Hvitved-Jacobsen, T., Vollertsen, J., 2005. Simulation of sulfide buildup in wastewater and atmosphere of sewer networks. Water Science and Technology 52 (3), 201–208.

Nielsen, A.H., Vollertsen, J., Hvitved-Jacobsen, T., 2006. Kinetics and stoichiometry of aerobic sulfide oxidation in wastewater from sewers-effects of pH and temperature. Water Environment Research 78 (3), 275–283.

Noguera, D., Okabe, S., Picioreanu, C., 1999. Biofilm modeling present status and future directions. Water Science and Technology 39 (7), 273–278.

Okabe, S., Nielsen, P.H., Charcklis, W.G., 1992. Factors affecting microbial sulfate reduction by *Desulfovibrio desulfuricans* in continuous culture: limiting nutrients and sulfide concentration. Biotechnology and Bioengineering 40 (6), 725–734.

Okabe, S., Ito, T., Satoh, H., 1999a. In-situ analysis of nitrifying biofilms as determined by in situ hybridization and the use of microelectrodes. Applied and Environmental Microbiology 65 (7), 3182–3191.

Okabe, S., Ito, T., Satoh, H., Watanabe, Y., 1999b. Analyses of spatial distributions of sulfate-reducing bacteria and their activity in aerobic wastewater biofilms. Applied and Environmental Microbiology 65 (11), 5107–5116.

Okabe, S., Ito, T., Satoh, H., 2003. Sulfate-reducing bacterial community structure and their contribution to carbon mineralization in a wastewater biofilm growing under microaerophilic conditions. Applied Microbiology and Biotechnology 63 (3), 322–334.

Petersen, B., Gernaey, K., Henze, M., Vanrolleghem, P.A., 2003. In: Agathos, S.N., Reineke, W. (Eds.), Biotechnology for the Environment: Wastewater Treatment and Modeling, Waste Gas Handling. Kluwer Academic Publishers, The Netherlands, Dordrecht, pp. 101–186.

Picioreanu, C., Kreft, J.U., van Loosdrecht, M.C.M., 2004. Particle-based multidimensional multispecies biofilm model. Applied and Environmental Microbiology 70 (5), 3024–3040.

Ramsing, N.B., Kuhl, M., Jorgensen, B.B., 1993. Distribution of sulfate-reducing bacteria, O_2, and H_2S in photosynthetic biofilms determined by oligonucleotide probes and microelectrodes. Applied and Environmental Microbiology 59 (11), 3840–3849.

Rauch, W., Vanhooren, H., Vanrolleghem, P.A., 1999. A simplified mixed-culture biofilm model. Water Research 33 (9), 2148–2162.

Satoh, H., Okabe, S., Yamaguchi, Y., Watanabe, Y., 2003. Evaluation of the impact of bioaugmentation and biostimulation by in situ hybridization and microelectrode. Water Research 37 (9), 2206–2216.

Sharma, K.R., Yuan, Z., de Haas, D., Hamilton, G., Corrie, S., Keller, J., 2008. Dynamics and dynamic modelling of H_2S production in sewer systems. Water Research 42 (10–11), 2527–2538.

Tsuno, H., Hidaka, T., Nishimura, F., 2002. A simple biofilm model of bacterial competition for attached surface. Water Research 36 (4), 996–1006.

Wanner, O., Gujer, W., 1986. A multispecies biofilm model. Biotechnology and Bioengineering 28 (3), 314–328.

Wanner, O., Reichert, P., 1996. Mathematical modeling of mixed-culture biofilms. Biotechnology and Bioengineering 49 (2), 172–184.

Wuert, S., Bishop, P.L., Wilderer, P.A., 2003. Biofilm in Wastewater Treatment. IWA Publishing, London.

Zhang, T.C., Bishop, P.L., 1994. Density, porosity, and pore structure of biofilms. Water Research 28 (11), 2267–2277.

Zhang, L., De Schryver, P., De Gusseme, B., De Muynck, W., Boon, N., Verstraete, W., 2008. Chemical and biological technologies for hydrogen sulfide emission control in sewer systems: a review. Water Research 42 (1–2), 1–12.